The Journal of Experimental Biology 202, 2433–2447 (1999)
Printed in Great Britain © The Company of Biologists Limited 1999
JEB2234

TAIL KINEMATICS OF THE CHUB MACKEREL *SCOMBER JAPONICUS*: TESTING THE HOMOCERCAL TAIL MODEL OF FISH PROPULSION

ALICE C. GIBB[1,*], KATHRYN A. DICKSON[1] AND GEORGE V. LAUDER[2,‡]

[1]*Department of Biological Science, California State University, Fullerton, CA 92834-6850, USA* and [2]*Department of Ecology and Evolutionary Biology, University of California, Irvine, CA 92697, USA*

*Present address: Department of Biological Sciences, Northern Arizona University, PO Box 5640, Flagstaff, AZ 86011, USA
‡Author for correspondence (e-mail: glauder@uci.edu); address from 1 October 1999: Museum of Comparative Zoology, Harvard University, Cambridge, MA 02138, USA

Accepted 14 July; published on WWW 25 August 1999

Summary

Scombrid fishes possess a homocercal caudal fin with reduced intrinsic musculature and dorso–ventrally symmetrical external and internal morphology. Because of this symmetrical morphology, it has often been assumed that scombrid caudal fins function as predicted by the homocercal tail model. According to that model, the caudal fin moves in a dorso–ventrally symmetrical manner and produces no vertical lift during steady swimming. To test this hypothesis, we examined the tail kinematics of chub mackerel, *Scomber japonicus* (24.8±1.3 cm total length, *L*). Markers were placed on the caudal fin to identify specific regions of the tail, and swimming chub mackerel were videotaped from lateral and posterior views, allowing a three-dimensional analysis of tail motion. Analysis of tail kinematics suggests that, at a range of swimming speeds (1.2–3.0 *L* s^{-1}), the dorsal lobe of the tail undergoes a 15 % greater lateral excursion than does the ventral lobe. Lateral excursion of the dorsal tail-tip also increases significantly by 32 % over this range of speeds, indicating a substantial increase in tail-beat amplitude with speed. In addition, if the tail were functioning in a dorso–ventrally symmetrical manner, the tail should subtend an angle of 90 ° relative to the frontal (or *xz*) plane throughout the tail beat. Three-dimensional kinematic analyses reveal that the caudal fin actually reaches a minimum *xz* angle of 79.8 °. In addition, there is no difference between the angle subtended by the caudal peduncle (which is anterior to the intrinsic tail musculature) and that subtended by the posterior lobes of the tail. Thus, asymmetrical movements of the tail are apparently generated by the axial musculature and transmitted posteriorly to the caudal fin. These results suggest that the caudal fin of the chub mackerel is not functioning symmetrically according to the homocercal model and could produce upward lift during steady swimming.

Key words: locomotion, swimming, tail function, Scombridae, *Scomber japonicus*, chub mackerel, kinematics.

Introduction

Teleost fishes typically possess a homocercal caudal fin with a symmetrical morphology in which the dorsal and ventral lobes of the tail fin are the same size and project posteriorly beyond the axis of the vertebral column. In contrast, most elasmobranch fishes and some primitive actinopterygian fishes possess a heterocercal caudal fin with an asymmetrical morphology in which the ventral lobe of the fin is smaller than the dorsal lobe and the vertebral column extends into the dorsal lobe of the fin. For over a century, it has been assumed that these morphological differences generate functional differences because the two types of tail should deflect water differently during steady swimming.

Early German morphologists (Schulze, 1894; Ahlborn, 1896) proposed that the asymmetrical morphology of the heterocercal tail creates asymmetrical water movement during the tail beat. According to the classic theory of heterocercal tail function, during the tail beat, the large, stiff upper lobe leads the smaller, flexible lower lobe, creating dorso–ventrally asymmetrical movements as the tail beats from side to side. The predicted consequence of this movement is that water is deflected ventrally as well as posteriorly during the tail beat, which creates an upward force, or lift, on the tail (Fig. 1). Support for this theory accumulated when experiments conducted using models (Grove and Newell, 1936; Affleck, 1950) and truncated elasmobranch caudal fins (Alexander, 1965) demonstrated that a heterocercal tail oscillated laterally produces upward lift under certain experimental conditions. More recently, Ferry and Lauder (1996) conducted the first comprehensive study of tail kinematics during steady swimming in a living elasmobranch (a leopard shark, *Triakis semifasciata*). Their study provides both three-dimensional kinematic data and flow visualization data that support the classic theory of heterocercal tail function. Therefore, this model appears to be accurate for some shark species, although it may not apply to all fishes that possess heterocercal tails (Lauder, 1999).

Unlike the heterocercal tail, the homocercal tail is symmetrical in morphology. Because of this symmetry, the homocercal tail has traditionally been assumed to produce no upward lift during steady swimming (Fig. 1). For example, in his classic paper on fish locomotion, Breder (1926; p. 225) states that in the homocercal tail "… there is no tendency to lift or depress the tail, the force being all in the horizontal plane". Similarly, Gosline (1971; pp. 35–36) notes that teleost fishes "… can swing both caudal lobes back and forth synchronously, both lobes generating a directly forward force". This view has also been supported by numerous other workers (e.g. Affleck, 1950; Patterson, 1968; review in Lauder, 1989).

However, surprisingly few researchers have examined the movements of the homocercal tail. Early research with tail models (Grove and Newell, 1936; Affleck, 1950) supported the theory that a homocercal tail moved from side to side produces no upward lift. Aleev (1969) noted that the caudal fin of many teleost fishes functions symmetrically during swimming, producing no lift, whereas the tail of other species may move at an acute angle to the direction of transverse tail movement. In the latter case, upward lift would be produced. However, Aleev (1969) did not provide a quantitative analysis of this phenomenon nor did he provide the references upon which he based his conclusions.

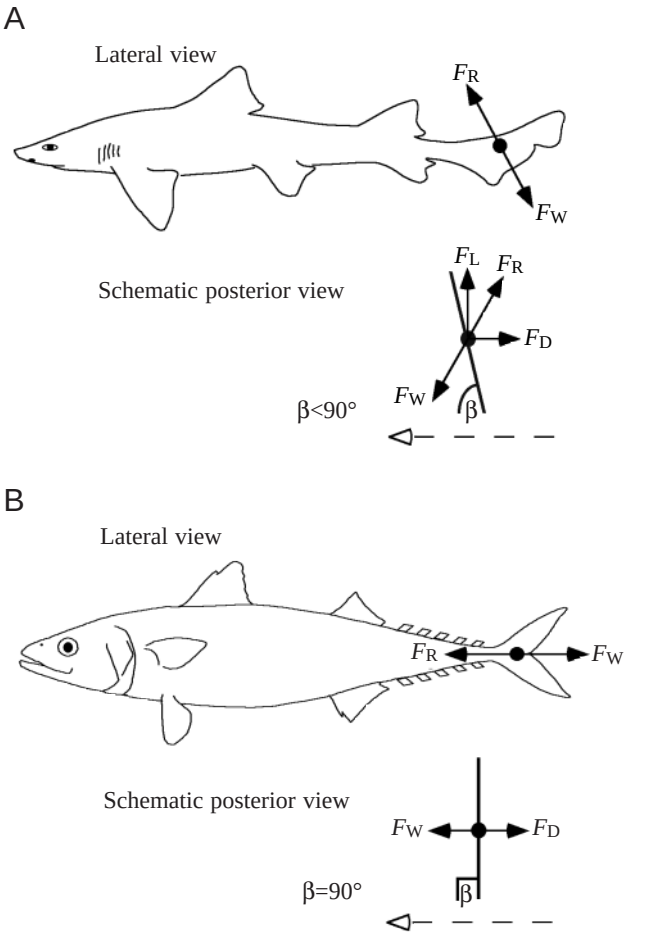

Fig. 1. Two models of tail function in fishes: (A) The classic model of heterocercal tail function in a shark; (B) the classic model of homocercal tail function in a mackerel. The angle of the fin relative to its direction of travel (β) is predicted to be less than 90° in the heterocercal model and equal to 90° in the homocercal model. F_L, lift force; F_D, drag force; F_R, resultant force; F_W, the force imparted to the water.

In the present study, we examine the caudal fin morphology and swimming kinematics of a derived actinopterygian fish, the chub mackerel *Scomber japonicus* (Teleostei: Scombridae). Scombrids are excellent fishes in which to examine the function of the homocercal tail for several reasons. First, they possess an internally and externally symmetrical caudal fin with reduced intrinsic tail musculature, stiff fin rays and a rigid caudal skeleton (Fierstine and Walters, 1968). Second, scombrids are thought to possess exceptional swimming performance (for a review, see Beamish, 1978) and swim continuously using their body and caudal fin. Finally, previous research on scombrid tail movements has provided evidence both supporting (Fierstine and Walters, 1968; Magnuson, 1970) and refuting (Aleev, 1969; He and Wardle, 1986) the classic model of homocercal tail function. However, all previous studies of scombrid swimming have been based on either qualitative observations or two-dimensional analyses (often for fish swimming in a circular tank or at very low speeds). Such analyses have recently been shown to be misleading (for a discussion of this problem, see Ferry and Lauder, 1996; Lauder and Jayne, 1996).

Therefore, the goal of the present study is to quantify the kinematics of the caudal fin in *Scomber japonicus* during steady swimming across a range of swimming speeds. A three-dimensional kinematic analysis will allow us to describe complex tail movements and to test the hypothesis that the tail of *S. japonicus* produces dorso–ventrally symmetrical movements during the tail beat. Finally, these results will be compared with similar studies recently conducted on a shark (Ferry and Lauder, 1996) and a more generalized teleost (Lauder, 1989, 1999) to determine what similarities and differences exist between the tail movements of mackerels and those of other fishes.

Materials and methods

Animal collection and maintenance

Scomber japonicus (Houttuyn) were captured off the coast of southern California, USA, using hook and line. Several fish were killed, fixed in 10% buffered formalin and subsequently used for morphological analysis. Other fish were transported to the laboratory and maintained in large (400–1000 l) saltwater aquaria with a 12 h:12 h light:dark photoperiod and fed daily on a diet of chopped frozen fish and squid. The four individuals (MK1, MK2, MK3 and MK4) videotaped for this study averaged 24.8±1.3 cm in total length, L (mean ± S.E.M., range 22–28 cm).

Morphological description

Specimens used for anatomical descriptions were stained by immersion in an Alizarin Red solution to identify the caudal bones. Preserved and stained specimens were dissected to determine whether *S. japonicus* possesses intrinsic tail muscles and to describe the location and orientation of those muscles.

Anatomical drawings were made using the dissected specimens, a Zeiss microscope with a *camera lucida* attachment, a graphics tablet, a Macintosh personal computer and a graphics program.

Experimental protocol

Prior to the experiments, individual fish were anesthetized in 0.1 g l^{-1} tricaine methanesulfonate (MS222) in salt water. When a fish stopped swimming because of the effects of the anesthesia, it was transferred into a shallow plastic tray filled with the anesthetic solution, and a peristaltic pump was used to pump oxygenated water continuously over the gills. The caudal fin was elevated out of the water to allow the attachment of small pieces of black labeling tape using cyanoacrylate adhesive. Three markers were placed in a vertical line just posterior to the caudal peduncle of the fish (Fig. 2). The most dorsal marker identified the mid-dorsal edge of the fin, the middle marker identified the central portion of the tail, and the most ventral marker identified the mid-ventral edge of the fin. Two sets of three markers were placed symmetrically on both sides of the caudal fin so that the same points could be identified on either side of the tail.

After marker attachment had been completed, the fish was placed into a large round tub containing oxygenated salt water and no anesthetic. This chamber was covered with dark plastic, and the fish was allowed to recuperate for a minimum of 60 min. At the end of the recovery period, the fish was quickly transferred to a flow tank maintained at a temperature of 19±1 °C and containing oxygenated salt water flowing at approximately 1 L s^{-1}. The fish was allowed to swim freely in the flow tank for another 30–60 min to allow it to adjust to the experimental chamber.

Following the adjustment period, the swimming fish was videotaped using a NAC HSV-500 high-speed video system, overhead photoflood lights and additional tungsten-flood or fiberoptic side lighting. A propeller and a variable-speed motor were used to adjust the water flow to the three target swimming speeds (1.2, 2.2 and 3.0 L s^{-1}) during videotaping. These speeds were chosen so that mackerel kinematic data could be compared with data collected for other fish species in previous work (Lauder, 1989, 1999; Ferry and Lauder, 1996). Mackerel were videotaped from lateral and posterior views simultaneously at the same absolute scale (Fig. 3), as in previous work (e.g. Ferry and Lauder, 1996). The lateral view was recorded with a video camera placed perpendicular to the front surface of the flow tank. The posterior view was recorded by a second video camera aimed at a front surface mirror located 0.5–1.0 L behind the swimming fish and positioned at 45° to the flow. Output from the two synchronized cameras was recorded as a split-screen image onto VHS videotape.

For one of the individuals used in this study, additional sequences of steady swimming at the three target speeds were videotaped. For these sequences, the lateral view was expanded so that the entire working area of the flow tank was visible. The second camera was used to observe the posterior view, and a split screen combining the two views was videotaped. The expanded lateral view was used to determine the angle of the body relative to the water flow during the tail-beat cycle. The posterior view was used to ensure that the fish was swimming in the center of the flow tank during these sequences. To obtain this view, additional light had to be focused on the anterior portion of the fish's body. The expanded lateral view was filmed for only one individual (MK3) because most individuals would not swim consistently at such high light levels.

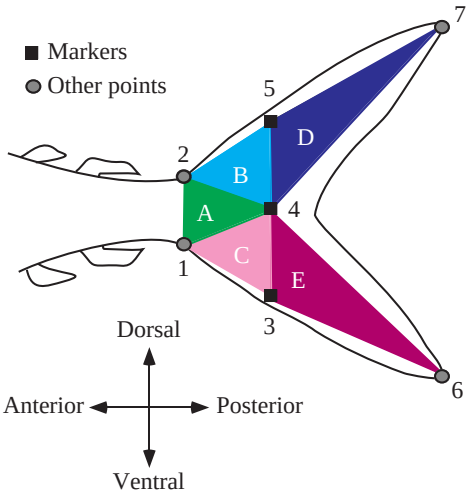

Fig. 2. A drawing of the tail of *Scomber japonicus* demonstrating: the seven points digitized (1–7), the orientation of these points relative to the body of the fish; and the five triangles (A–E) that can be constructed on each tail using the three-dimensional coordinates of the points.

Kinematic analysis

Video images were analyzed using a Peak Performance motion-analysis system. Four tail beats were analyzed for each individual at each swimming speed. In most cases, four sequential tail beats were chosen; however, in a few cases, two sets of two sequential tail beats were combined. Only sequences in which the fish was matching swimming speed with the water flow, swimming in the approximate center of the tank (away from the tank walls, tank bottom and water surface), and not drifting vertically or laterally were chosen for kinematic analysis.

Swimming sequences were recorded at 250 fields s^{-1} and then down-sampled to approximately 20 fields tail $beat^{-1}$. Because the tail beats at a different frequency at each swimming speed, a different sampling rate was used for each speed. At 1.2 L s^{-1}, the sampling rate was one field every 20 ms, at 2.2 L s^{-1}, one field every 16 ms, and at 3.0 L s^{-1}, one field every 12 ms.

All three tail markers were digitized in the lateral and posterior views for each field. In addition, four other easily identifiable points on the tail were digitized: the two posterior tail-tips and the dorsal and ventral junctions of the fin rays with the caudal peduncle (Fig. 2). Finally, a reference point in the flow tank was digitized in each field for both views so that

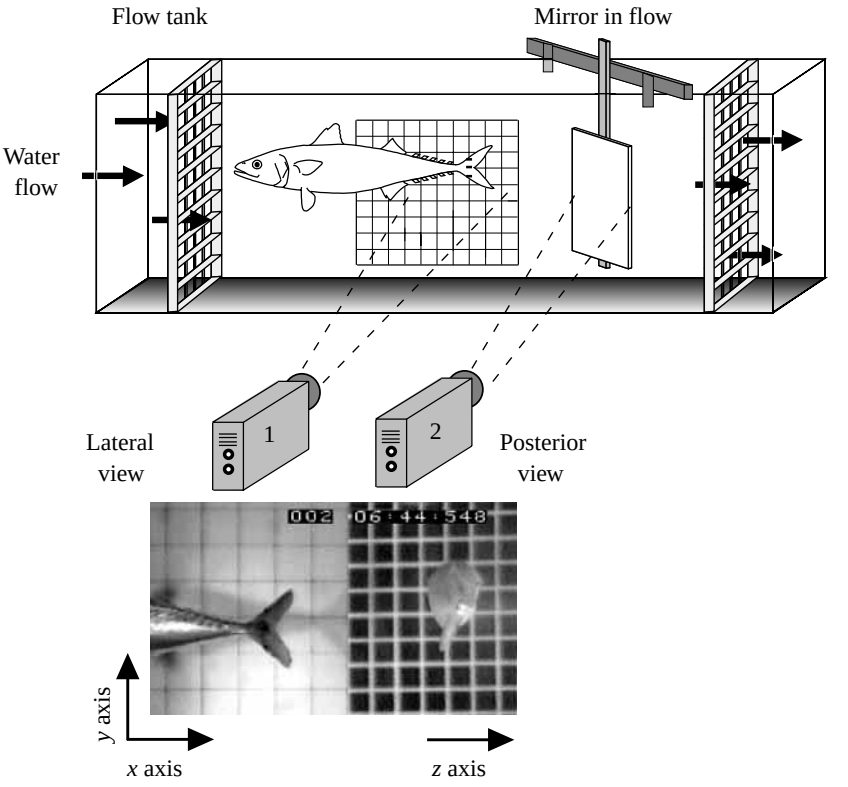

Fig. 3. Schematic drawing of the flow tank and videotaping methods. The mackerel is shown swimming in the working section of the flow tank with a mirror positioned downstream. Two cameras simultaneously record lateral and posterior views as a split-screen high-speed video image, allowing a three-dimensional reconstruction of tail movements. Note that the size of both the mackerel and the mirror are considerably enlarged in this schematic figure relative to their size in the actual experimental apparatus.

movements of the tail could be quantified relative to an external frame of reference. These data provided the lateral (*z*), vertical (*y*) and horizontal (*x*) positions of the seven points on the tail during the fin-beat (Fig. 3).

After digitizing, coordinates from the points on the tail were exported to a computer spreadsheet program, and kinematic displacement and timing variables were calculated for each tail-beat cycle. To quantify displacement, the excursion (maximum position − minimum position) of each of the seven tail points was measured in all three dimensions for each tail beat.

Timing variables were also measured for *z* (lateral) movements. Maximum lateral excursion of the dorsal tail-tip was used to measure tail-beat frequency (in Hz). The time (in seconds) of maximum *z* (lateral) displacement was measured for every point on the caudal fin. Time lags were calculated by subtracting the time of maximum lateral displacement of the dorsal tail-tip from the time of maximum lateral displacement for each of the other six points on the tail. Thus, points that achieved maximum displacement before the dorsal tail-tip had negative time lags, and those that achieved maximum displacement after the dorsal tail-tip had positive time lags. Time lags varied with tail-beat frequency (i.e. a high-frequency tail beat always has small time lags when measured in seconds). Consequently, each time lag was divided by the time it took the tail to complete that particular tail-beat cycle; this yielded phase lag, a measure of time lag as a percentage of tail-beat cycle time. Because data calculated as ratios are not normally distributed, the phase lag data were transformed using an arcsine transformation before statistical analyses were performed (Zar, 1984).

Three-dimensional angle calculations

As in previous work (e.g. Ferry and Lauder, 1996), kinematic data were filtered to remove small variations created by digitizing error before they were used for three-dimensional analysis. Filtering was accomplished using the binomial smooth function (with two passes) in the program Igor (version 3.3) for the Macintosh personal computer. From the smoothed data set, the seven points digitized on the tail were used to create three-dimensional triangles representing surface elements of the tail (Fig. 2). Following methods previously described in Lauder and Jayne (1996), the coordinates (*x*, *y*, *z*) for each of three points defining a triangle on the tail were used to calculate the orientation of the three-dimensional plane representing each triangle (Fig. 4). Three reference planes were defined by the *x*, *y* and *z* dimensions. The *xz* or frontal plane is parallel with the bottom of the flow tank, the *xy* or parasagittal plane is parallel with the back wall of the flow tank, and the *yz* or transverse plane is parallel with the front baffle of the flow tank (Fig. 4). The angles of intersection of the tail triangle planes with each of these three reference planes were then calculated. Intersection of the triangle plane with the *yz* and *xz* planes was defined relative to 90 ° and the intersection with the *xy* plane was defined relative to 0 °. For example, if a tail triangle were positioned at 90 ° relative to the *yz* and *xz* planes and at 0 ° relative to the *xy* plane, it would be a simple vertical plane, entirely parallel to the back wall and the path of water flow through the flow tank.

Three-dimensional angle calculations were used to quantify movements of particular regions of the tail over time and to test specific hypotheses about tail function. If the tail of *S.*

japonicus functions as predicted by the homocercal model, then a point on the dorsal lobe of the tail should have the same *x* (horizontal) and *z* (lateral) coordinates as the homologous point on the ventral lobe of the tail throughout the tail beat. If this is the case, then any given region of the tail will consistently maintain an angle of 90 ° relative to the *xz* plane and be perpendicular to the bottom of the flow tank (see angle β for the homocercal model in Fig. 1).

Even if the first hypothesis is rejected, a second type of dorsal–ventral symmetry can be assessed. If the dorsal and ventral lobes of the tail are not at an orientation of 90 ° in the *xz* plane, they could still be symmetrical in another manner. If the two lobes are moving symmetrically about the dorsal midline of the fish, then the tail triangles of the upper and lower lobes should actually have opposite orientations. For example, if the dorsal lobe is at 80 ° relative to the path of travel of the tail, then the ventral lobe should be at 110 ° (in this example, each lobe is deflected 10 ° away from the peduncle). Thus, comparing the *xz* planar angles of homologous tail triangles in the dorsal and ventral lobes of the tail (e.g. triangles D and E, Fig. 2) will determine whether the dorsal and ventral lobes of the tail move symmetrically about the mid-line during the tail beat.

During each tail beat, the caudal fin achieves a maximum and a minimum angle in each plane. The maximum and minimum angles for each beat were determined for individual tail triangles. These values were subtracted from the reference value for each plane (0 ° for *xy* and 90 ° for *yz* and *xz*). The absolute value of this difference was used to calculate the maximum deviation from the reference value in each plane. The timing of these angular changes was determined relative to the tail-beat cycle by calculating the phase lag between angular movements of triangles and the displacement of the dorsal tail-tip. As described above for the displacement data, angular phase lags were calculated as a percentage of tail-beat cycle time and arcsine-transformed prior to statistical analysis.

A subsample of the data set was analyzed using three-dimensional angle calculations. Only the highest and lowest swimming speeds were compared for the planar angles in all four mackerel; the middle speed was not examined because the kinematics at this speed were not statistically different from the kinematics at the other two speeds (see Results). In addition, preliminary analysis of the *xy* and *yz* angles indicated that all tail triangles achieve approximately the same maximum/minimum angle and have similar timing (see Fig. 11). Therefore, the timing (relative to the tail-beat cycle) and absolute magnitude of the angular movements of triangle D (Fig. 2) were measured in the *xy* and *yz* planes from all fish at both speeds to summarize overall tail movements in these two planes.

The preliminary analysis of movements in the *xz* plane indicated that the tail triangles might vary in both angle magnitude and relative timing (see Fig. 12). However, the two dorsal tail triangles (see Fig. 12, triangles B and D) showed very similar patterns of movement, as did the two ventral tail triangles (Fig. 12, triangles C and E). Because of the similarities between these two sets of triangles, only the movements of triangles A, D, and E were statistically examined for the *xz* plane.

Statistical analyses

Statistical analyses were performed on the data using the programs StatView (version 4.5) and SuperANOVA (version 1.11) for the Macintosh. The preliminary analysis of the *x*, *y* and *z* excursion variables was a three-way multivariate analysis of variance (MANOVA), for which the main effects were speed, location and individual. In this analysis, speed and location were considered to be fixed effects and individual was considered to be a random effect. The *F*-value for the individual effect was calculated as the mean square (MS) individual divided by the MS residual. *F*-values for fixed factors were calculated as the MS of the fixed effect divided by the two-way interaction term of the random (individual) effect and the fixed effect. The *F*-values for the two-way interaction terms for fixed and random effects (location × individual and speed × individual) were calculated using the MS residual. Finally, the *F*-value for the two-way interaction of the two fixed effects (location × speed) was determined using the three-way interaction term (location × speed × individual) (Zar, 1984). When the results of the MANOVA indicated that there was significant variation in the data set due to some of these effects, separate three-way analyses of variance (ANOVAs) were performed on the *x*, *y* and *z* displacements to determine which of these variables showed individual, speed, location or interaction effects. Error terms for the *post-hoc* three-way ANOVAs were calculated as described above for the MANOVA, although only effects found to be significant in the MANOVA were considered. Tukey–Kramer *post-hoc* tests were performed on each variable that showed significant speed and/or location effects in the three-way ANOVAs.

Timing variables were considered in a separate series of statistical tests. A two-way ANOVA was performed on the tail-beat frequency data considering the possible effects of individual, speed and the interaction term (individual × speed). In this ANOVA, speed was again considered as a fixed effect and the *F*-value was calculated as the MS of speed divided by the MS of individual × speed. Individual and interaction effects were calculated using the residual MS.

The timing of maximum lateral displacement of the various points on the tail relative to the tail-tip (phase lag) was analyzed using one-sample *t*-tests and an additional three-way ANOVA. (Phase lag could not be included in the MANOVA described above because there are no data for the phase lag of the point on the dorsal tail-tip relative to itself.) A series of one-sample *t*-tests determined which phase lags differed significantly from the null hypothesis that there was no phase lag. *F*-values for the three-way ANOVA on phase lags were calculated as described above for the displacement variable MANOVA and ANOVAs. Tukey–Kramer *post-hoc* tests were performed on any significant speed and/or location effects.

Another three-way MANOVA was used to analyze the magnitude and timing variables of the *xz* angle for triangles A, D and E. The effects and error terms for this MANOVA were

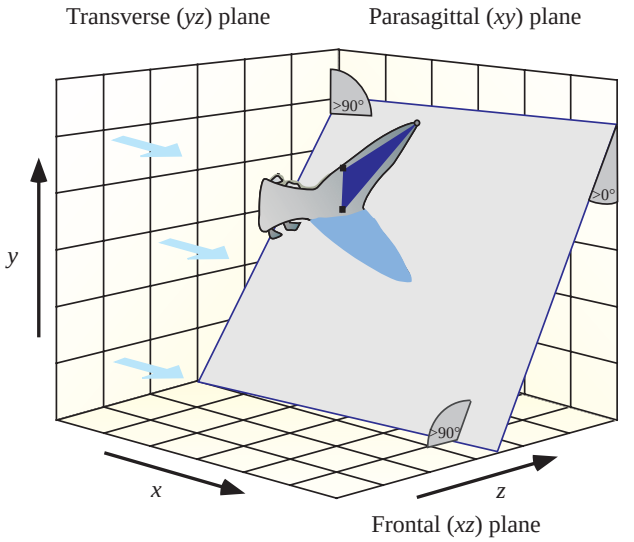

Fig. 4. Schematic illustration of the mackerel tail in three-dimensional space to show the three-dimensional angle orientations and conventions. Three reference planes are defined by the *x*, *y* and *z* dimensions. (1) The *xz* (frontal) plane is parallel with the bottom of the flow tank. (2) The *xy* (parasagittal) plane is parallel with the back wall of the flow tank. (3) The *yz* (transverse) plane is parallel with the front baffle of the flow tank (see Fig. 3). Three-dimensional coordinates for a tail triangle can be used to calculate a plane that intersects with the reference planes to form three angles: *xz*, *xy* and *yz* angles. In this image, the upper-posterior triangle of the tail (triangle D) forms a plane that is shown intersecting with the three reference planes; the lower lobe of the tail is not parallel with this plane at that point in time. The light blue arrows to the left represent the direction of water flow through the tank. See Materials and methods for a more complete description of these calculations.

calculated as described above for the displacement variables. Again, terms that were not significant in the MANOVA were not included in the subsequent three-way ANOVAs, and Tukey–Kramer *post-hoc* tests were used to determine which triangles differed from one another.

Additional kinematic variables

Using the posterior view of all swimming sequences, a qualitative assessment was made of the degree of abduction of the pectoral fins during the tail-beat cycle. This was performed to determine whether the orientation of the pectoral fins changes with swimming speed. The angular orientation of the pectoral fin was not quantified because it could not be measured without the use of an additional camera view (a dorsal or ventral view) of the swimming fish.

The expanded lateral view videotaped for one individual (MK3) was used to calculate the orientation of the fish's body relative to the flow. The path of travel of the flow was estimated using a horizontal line that formed part of the grid on the back wall of the flow tank (Figs 3, 4); these lines are parallel to the water flow through the working section of the tank. A line measured from the tip of the fish's snout to the fork in the caudal fin was used to describe the orientation of the fish's body. The intersection of these two lines defined the angle of the fish's body relative to the flow. This angle was measured for ten fields spanning two complete tail-beat cycles at each of the three swimming speeds.

Results

Tail morphology

Two intrinsic tail muscles were found in dissected specimens of *S. japonicus* after the tendons from the axial musculature had been reflected anteriorly (Fig. 5). The interradialis muscle originates on the most medial fin rays, just posterior to the hypural plate, and inserts on the medial surface of more distal caudal fin rays. This muscle is positioned such that it should compress the tail vertically when it contracts. A

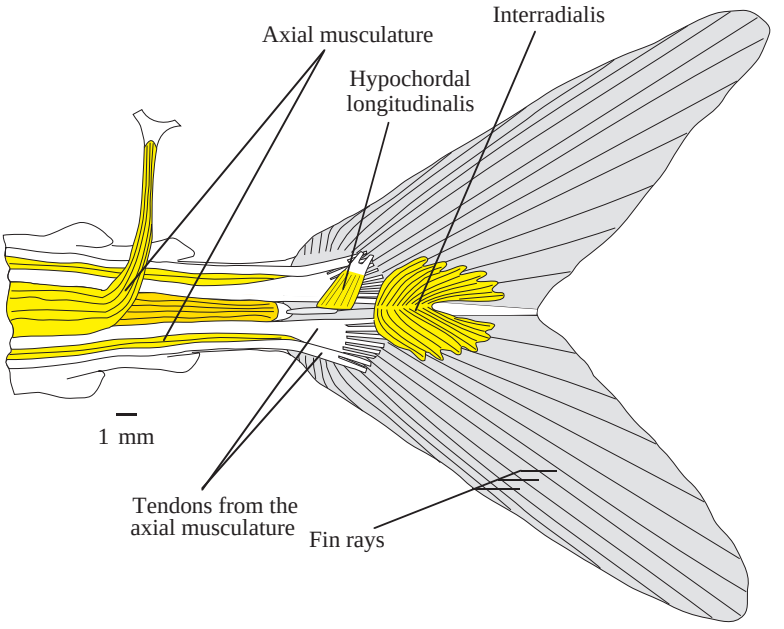

Fig. 5. The tail of a preserved *Scomber japonicus* illustrating the intrinsic muscles of the caudal fin. The axial musculature has been reflected anteriorly to reveal the deep muscles of the tail. Note the relative size and orientation of the hypochordal longitudinalis muscle.

smaller muscle is also present in the tail: the hypochordal longitudinalis (HL). The HL originates on the hypural plate and inserts on the longest dorsal fin rays (Fig. 5). It is positioned such that contraction of this muscle should move the dorsal rays of the tail laterally relative to the ventral rays. Although the deep ventral flexor has been reported previously in sierra mackerel *Scomberomorus* sp. (Nursall, 1963), it was not observed in the caudal fin of *S. japonicus*.

Orientation of the body and pectoral fins

Qualitative assessment of the angle of the pectoral fins to the body suggests that both pectoral fins were abducted more at lower swimming speeds. At higher swimming speeds, the pectoral fins are adducted and positioned closer to the body. At all the swimming speeds, the pectoral fins were somewhat abducted; at no time were they held flush against the body.

Body angle was slightly negative at all swimming speeds for the one individual measured. The mean body angles for the individual measured were –0.5±0.09 ° at 1.2 $L\,s^{-1}$, –2.1±0.09 ° at 2.2 $L\,s^{-1}$ and –0.5±0.13 ° at 3.0 $L\,s^{-1}$ (means ± S.E.M.). A consistently positive body angle of attack was never observed in any of the four mackerel used in this study.

General tail-beat kinematics

During the tail-beat cycle, there was relatively little movement in the *y* (vertical) and *x* (horizontal) dimensions (Fig. 6); the majority of the tail movement occurred in the *z* (lateral) dimension as the tail beat from side to side. Although very little movement occurs in the *y* dimension, the movement that did occur was greatest at the tail-tips. In fact, the tail underwent a cyclic vertical expansion and compression (Fig. 7). Even though tail height varied from cycle to cycle, the tail was consistently at its maximum expansion mid-beat (as the tail crossed the midline of the direction of travel). In contrast, the tail was maximally compressed at the maximum lateral displacement of the tail-tip, as the tail reversed direction.

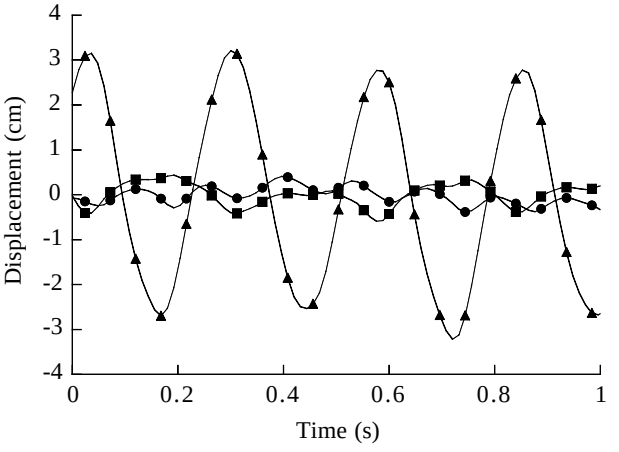

Fig. 6. Three and a half tail beats measured from a mackerel (MK1) swimming at 3.0 $L\,s^{-1}$. The lines represent movements of the dorsal tail-tip of the fin in three dimensions (*x*, *y* and *z*). Only every fourth data point is shown as a marker on the line for clarity. ●, *x* (horizontal) movements; ■, *y* (vertical) movements; ▲, *z* (lateral) movements. All variables show a cyclic pattern of change, but the magnitude of change is largest in the *z* (lateral) dimension.

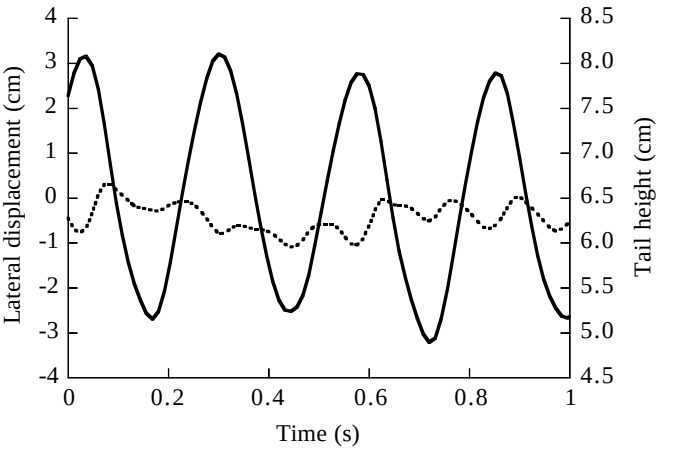

Fig. 7. Three and a half tail beats measured from a mackerel (MK1) swimming at 3.0 $L\,s^{-1}$. The solid line represents movements in the *z* (lateral) dimension. Note that the left and right *y*-axes are shown at different scales. The dashed line represents changes in the height of the tail as measured from the dorsal and ventral tail-tips. Although there is some variability in overall tail height, it is consistently greatest when the tail-tip crosses the mid-line of its path of travel (i.e. *z*=0) and smallest when the tail is maximally laterally displaced.

Examination of individual tail beats revealed that dorso–ventral asymmetry was present in the lateral movements of the tail. The lateral excursion of the dorsal portion of the tail was consistently greater than the lateral excursion of the ventral portion of the tail (Fig. 8). This result suggests that the dorsal lobe ‘leads’ the ventral lobe during the tail beat.

Displacement variables

The MANOVA of the three-dimensional displacement variables (*x*, *y* and *z*) indicated that only lateral (*z*) excursions

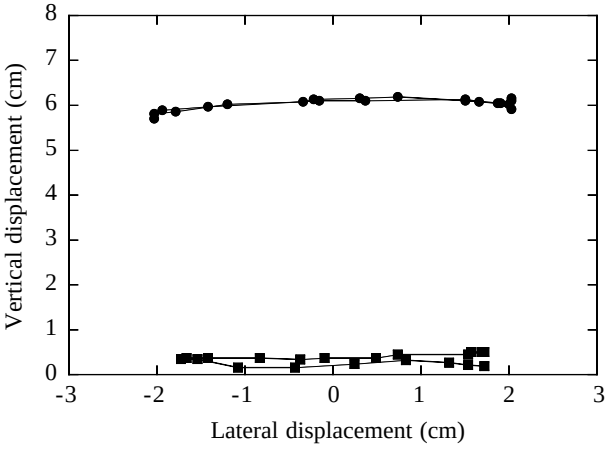

Fig. 8. One tail beat measured from a mackerel (MK4) swimming at 3.0 $L\,s^{-1}$. ●, movements of the dorsal tail-tip; ■, movements of the ventral tail-tip. The dorsal tail-tip undergoes a greater excursion (greater than 4 cm) during the tail beat than does the ventral tail-tip (less than 4 cm). These data are typical for all individuals at all swimming speeds.

Table 1. *Results (*F*-values) of three separate three-way ANOVAs on* x, y *and* z *displacement variables*

Variable	Individual	Speed	Location	Individual× speed
d.f.	3, 318	2, 6	6, 318	6, 318
x	11.3*	3.2	6.3*	16.6*
y	36.9*	0.7	14.0*	18.2*
z	122.9*	10.4*	144.2*	33.4*

d.f., degrees of freedom.
*Statistical significance at $P<0.05$.

showed significant speed effects, indicating that tail-beat amplitude increases with speed. There were also significant effects of individual (*F*-value 46.6, Wilks' lambda <0.001), speed (*F*-value 8.0, Wilks' lambda <0.05), location (*F*-value 9.7, Wilks' lambda <0.001), and individual × speed (*F*-value 18.1, Wilks' lambda <0.001). There was no significant effect of the other two-way interaction terms or the three-way interaction term (in all cases *F*-value <2, Wilks' lambda >0.10); thus, these terms were eliminated from subsequent statistical analyses. The three-way ANOVAs conducted as *post-hoc* tests revealed that *x* (horizontal), *y* (vertical) and *z* (lateral) movements all demonstrated effects of individual, location and individual × speed (Table 1).

Tukey–Kramer *post-hoc* tests determined which locations on the tail could be statistically distinguished from one another. When all three variables are considered together, it is clear that four points (the dorsal and ventral peduncle and the ventral and central mid-tail) cannot be distinguished from one another in any dimension (points 1–4, Fig. 9) and therefore demonstrate similar kinematics. In addition, the amplitude of the excursions in all three dimensions tends to be smallest in the peduncle and mid-tail regions and larger at the tail-tips (Fig. 9; Table 2), although this trend is least apparent for the *x* (horizontal) dimension.

The tail also demonstrated dorso–ventral asymmetry. This result was highly significant in the *z* (lateral) dimension, where the excursion of the dorsal tail-tip was 15 % larger than that of the ventral tail-tip, and the excursion of the dorsal mid-tail was 9 % greater than that of the central mid-tail (Fig. 9; Table 2). *x* (horizontal) and *y* (vertical) average excursions were quite small. In contrast, the average excursions for the *z* (lateral) dimension were almost an order of magnitude larger (Fig. 9). Tail-beat amplitude (as measured by the lateral excursion of the dorsal tail-tip) increased by 32 % from 1.2 to 3.0 $L\,s^{-1}$, and this reflects the substantial speed effects observed for the tail *z* excursions (Tables 1, 2).

Lateral (*z*) excursion was the only displacement variable that showed a speed effect in the three-way ANOVA. Since there

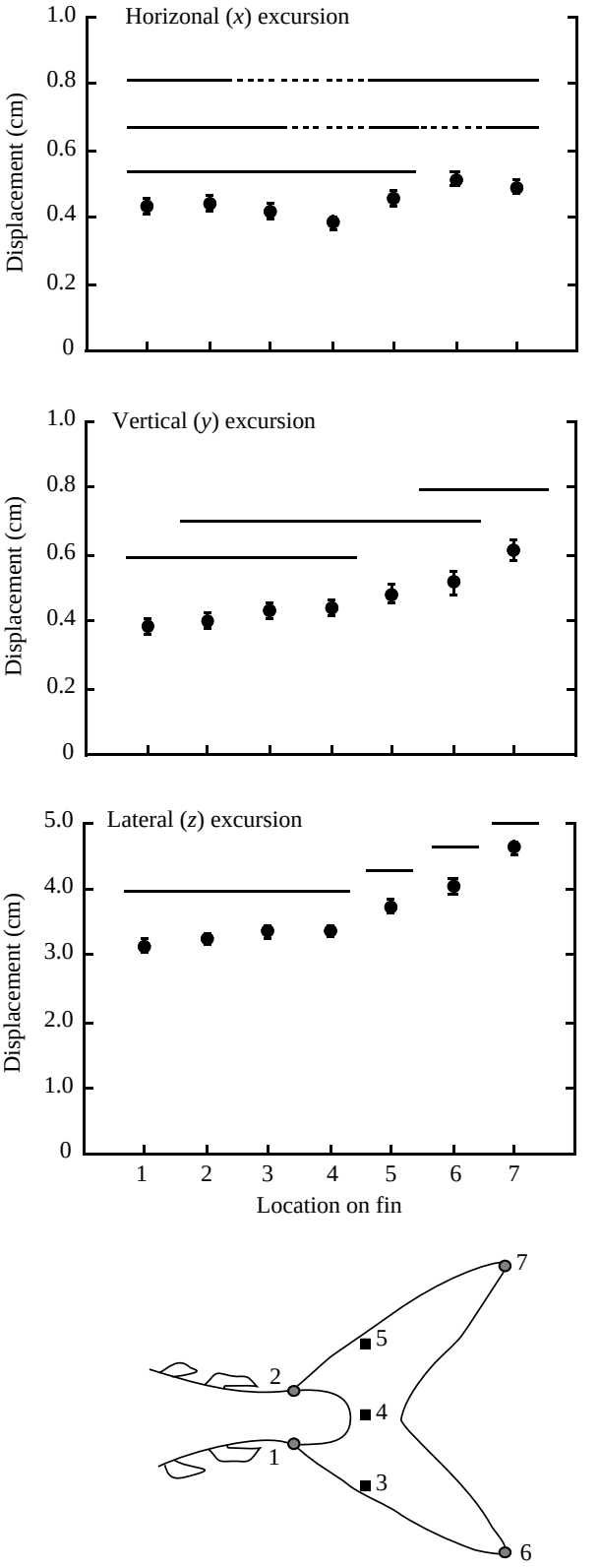

Fig. 9. Mean excursion values (± S.E.M.) for all individuals at all swimming speeds, illustrating the effect of fin location on amplitude of movement in all three dimensions (*N*=48 for each point). The location points digitized on the tail are: 1, ventral peduncle; 2, dorsal peduncle; 3, ventral mid-tail; 4, central mid-tail; 5, dorsal mid-tail; 6, ventral tail-tip; 7, dorsal tail-tip; a schematic drawing of the tail (bottom) is shown for reference. Horizontal lines represent locations on the tail that could not be distinguished statistically from one another using Tukey–Kramer *post-hoc* tests. A dashed line indicates that the location below the dash was not included in a particular statistical grouping.

Table 2. z *(lateral) excursions for all individuals shown for each swimming speed and each location on the tail*

	Speed ($L\,s^{-1}$)		
Variable	1.2	2.2	3.0
Ventral peduncle (cm)	2.64±0.12	3.22±0.09	3.58±0.12
Dorsal peduncle (cm)	2.77±0.12	3.31±0.09	3.68±0.13
Ventral mid-tail (cm)	2.76±0.13	3.48±0.09	3.81±0.12
Center mid-tail (cm)	2.83±0.11	3.47±0.09	3.83±0.09
Dorsal mid-tail (cm)	3.16±0.13	3.87±0.11	4.20±0.14
Ventral tail-tip (cm)	3.39±0.15	4.20±0.17	4.52±0.16
Dorsal tail-tip (cm)	3.91±0.14	4.75±0.15	5.17±0.16
N	16	16	16

Values are means ± S.E.M.

was no significant interaction of location × speed in the MANOVA, the *z* excursions for all locations can be considered together. In general, the *z* excursion of the tail increased with swimming speed; at $1.2\,L\,s^{-1}$, overall *z* excursion was 3.1±0.1 cm, at $2.0\,L\,s^{-1}$, 3.8±0.1 cm and, at $3.0\,L\,s^{-1}$, 4.1±0.1 cm (means ± S.E.M.). *Post-hoc* tests revealed that the average lateral excursions for the points on the tail were significantly different from one another at the lowest and highest speeds. However, the middle swimming speed could not be distinguished statistically from either the highest speed or the lowest speed when all points on the tail are considered together. The significant interaction effect of individual × speed can be attributed to the fact that, although all individuals increased *z* excursion with swimming speed, some individuals increased *z* excursion of the tail more than others.

Timing variables

The two-way ANOVA revealed that there was significant variation in tail-beat frequency due to individual (*F*-value 10.9, $P<0.001$), speed (*F*-value 53.2, $P<0.001$) and individual × speed effects (*F*-value 3.0, $P<0.05$). Tail-beat frequency increased linearly with swimming speed; at $1.2\,L\,s^{-1}$, tail-beat frequency was 2.4±0.08 Hz, at $2.2\,L\,s^{-1}$, 3.0±0.08 Hz and at $3.0\,L\,s^{-1}$, 3.7±0.05 Hz. *Post-hoc* tests revealed that all three speeds could be distinguished statistically from one another for this variable. The significant interaction effect of individual × speed can be attributed to the fact that some individuals increased tail-beat frequency more rapidly than others.

Phase lags for each of the six points were determined to be significantly different from zero in the one-sample *t*-tests (for all six tests, *t*-value >4.0, $P<0.001$). The three-way ANOVA performed on the phase-lag variables indicated that there were significant individual (*F*-value 6.0, $P<0.001$), location (*F*-value 5.2, $P<0.05$) and individual × location (*F*-value 2.6, $P<0.05$) effects. There was no significant effect of the other two-way interaction terms or the three-way interaction term (in all cases *F*-value <2, $P>0.10$).

In general, the wave of lateral displacement was propagated posteriorly, as expected. For example, the ventral and dorsal peduncle points reached their maximum lateral displacements approximately 9 % of the total cycle time ahead of the dorsal tail-tip. In addition, dorso–ventral asymmetry in the timing of tail movements was apparent. The ventral tail-tip reached its maximum lateral displacement approximately 3 % of the cycle time behind the dorsal tail-tip (Fig. 10). Although the magnitude of this response varied among individuals (creating an individual × location effect), the same general trend was present in all of the individuals.

Three-dimensional orientation

Planar angle calculations revealed that the tail oscillated in all three reference planes throughout the tail beat. The *yz* angle underwent relatively simple changes. Triangle D cycled 21±1.0 ° (mean ± S.E.M.) above and below 90 °, and the other triangles showed a similar pattern (Fig. 11). This cycle is approximately 16.1±1 % out of phase with the cycle of lateral displacement of the dorsal tail-tip when all individuals at both speeds were considered. Consequently, the *yz* angle was at its minimum angle shortly before the tail crossed the mid-line of its path of travel (70 % cycle time, Fig. 11C). The *yz* angle was 90 ° (and therefore perpendicular to that plane) shortly before

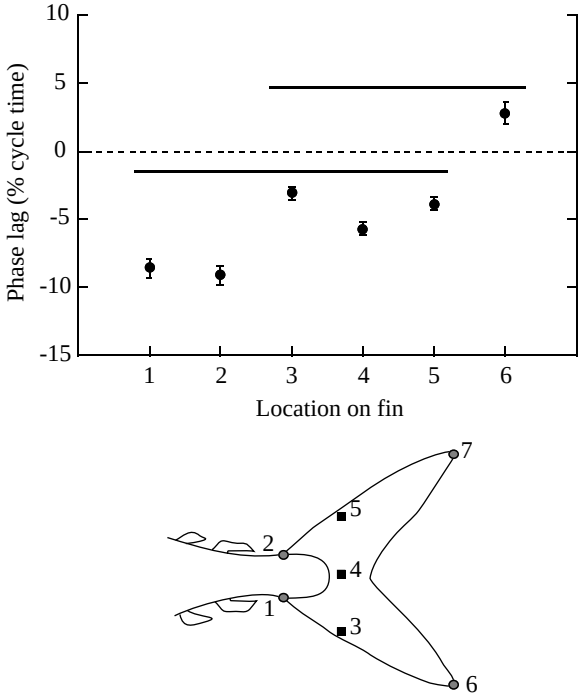

Fig. 10. Mean phase lag (± S.E.M.) measured as a percentage of tail-beat cycle time for all individuals at all swimming speeds, illustrating the effect of location on the fin on the timing of lateral (*z*) movements of the fin. The locations on the tail are numbered as in Fig. 9; a schematic drawing of the tail is shown for reference. The dorsal tail-tip phase lag is not shown because it is the location used to determine the timing of the tail-beat cycle and is zero by definition. A negative value indicates that the point reached its maximum lateral displacement before the dorsal tail-tip; a positive value indicates that the point reached its maximum lateral displacement after the doral tail-tip. Horizontal lines over the values represent locations that could not be distinguished statistically from one another using Tukey–Kramer *post-hoc* tests.

it reached maximum lateral displacement (90 % cycle time, Fig. 11C). At that point, the tail triangle was parallel to the path of water flow through the tank. All six triangles in the tail were in a similar orientation to one another throughout the beat, although the magnitude of the angle subtended by each triangle in this plane varied slightly.

Movements of the tail in the *xy* plane showed a similar pattern to that seen for *yz* angle. The *xy* angle of triangle D oscillated 20.8±1 ° (mean ± S.E.M.) above and below 0 ° during the tail-beat cycle (Fig. 11B). Interestingly, the phase lag for the *xy* angle relative to the movements of the dorsal tail-tip was also the same (16.6±1 %) as that observed for the *yz* angle. In this instance, tail triangles were parallel to the parasagittal plane (0 °) shortly before the tail reached its maximum lateral displacement. Again, all six tail triangles were similar in orientation throughout the tail beat. These data (and the *yz* angle data) suggest that the anterior and posterior regions of the tail were aligned in the horizontal axis near the end of a tail beat and were not aligned mid-beat.

The pattern for the *xz* angle was quite different in several ways. First, not all the tail triangles showed the same pattern (Fig. 12). Consequently, the phase relationships (relative to tail-tip movements) differed for the different tail triangles. However, changes in the *xz* orientation of the two dorsal tail triangles (triangles B and D) were quite similar, as were changes in the *xz* orientation of the two ventral tail triangles (triangles C and E; Fig. 12). Because of the similarities between the two dorsal and two ventral triangles, only the caudal peduncle (triangle A) and the posterior triangles (D and E) were examined statistically (see Materials and methods).

The MANOVA revealed that there was significant variation in the *xz* angle magnitude and timing data due to the effects of individual (*F*-value 11.4, Wilks' lambda <0.001), location (*F*-value 15.4, Wilks' lambda <0.001), individual × location (*F*-value 4.5, Wilks' lambda <0.001), and individual × speed (*F*-value 3.8, Wilks' lambda <0.05). There was no significant speed effect and no other interaction terms were significant (in all cases, *F*-value <3, Wilks' lambda >0.05); these terms were therefore eliminated from subsequent statistical analyses. Three-way ANOVAs indicated that the timing variables for the *xz* angle showed significant effects for each of the terms found to be significant in the MANOVA, including an effect of location on the fin (Table 3). Tukey–Kramer *post-hoc* tests revealed that the timing of movements of triangle D was significantly different from that of triangles A and E. The magnitude of the *xz* angle showed no significant location effect, but the other three terms (individual and the interaction terms) were significant (Table 3).

The average maximum/minimum angle for triangles A, D and E in the *xz* plane was 10.2±0.5 ° (mean ± S.E.M.) above or below 90 °. When the direction of movement of the tail is taken into account, these values indicate that the caudal fin consistently subtended an acute angle relative to its direction of travel during the fin beat. However, the magnitude of this angle oscillated as the tail beat. Triangles A (the peduncle) and E (the ventral lobe) were 21±1 % (mean ± S.E.M.) ahead of the

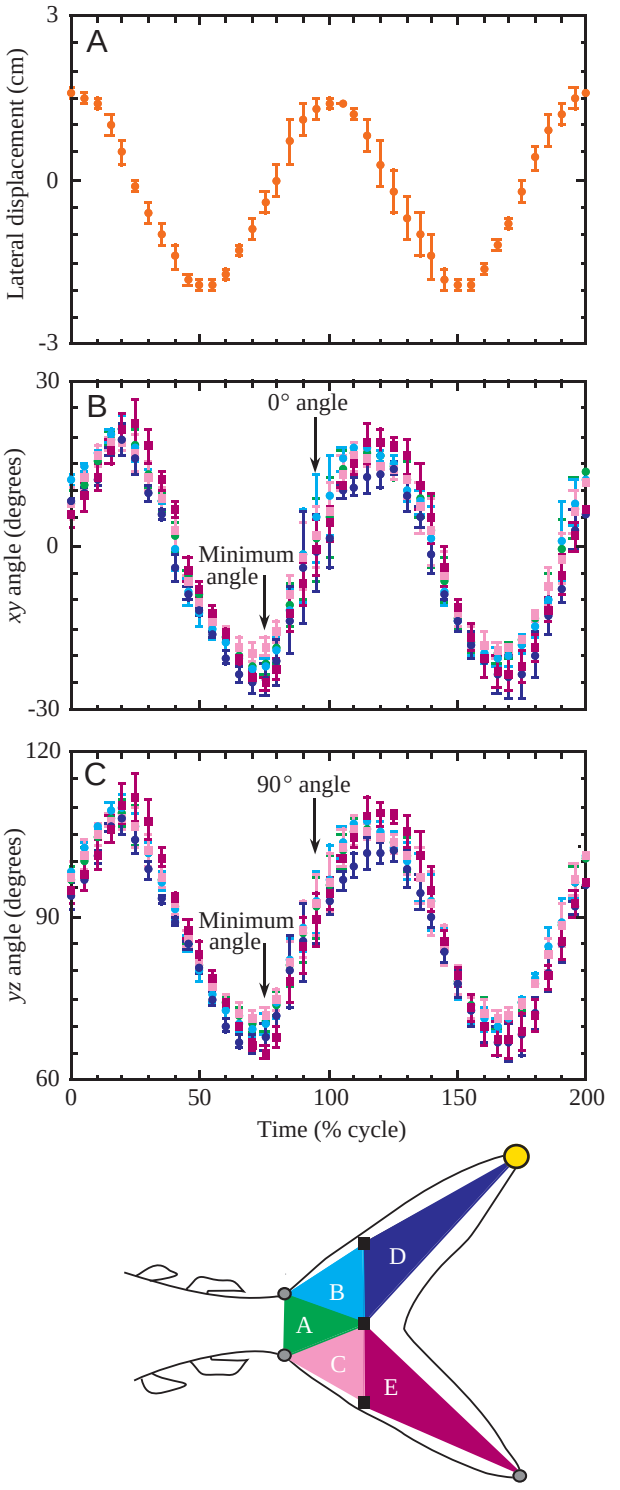

Fig. 11. Orientation of tail triangles in the *xy* and *yz* planes and lateral displacement of the tail-tip during the tail-beat cycle. Points represent the mean values (±S.E.M.) for all individuals swimming at the lowest swimming speed (1.2 $L\,s^{-1}$) for two complete tail beats. (A) Lateral displacement of the tail-tip, (B) *xy* angle of all tail triangles and (C) *yz* angle of all tail triangles. The tail-tip displacement is 0 cm as the tail crosses the mid-line of its path of travel. Markers on the graphs are color-coded to match the tail triangles.

Table 3. *Results (F-values) of three three-way ANOVAs on* xz *angle magnitude and relative timing*

Variable	Individual	Location	Individual× location	Individual× speed
d.f.	3, 79	2, 6	6, 79	5, 79
xz angle	21.5*	2.8	4.1*	10.1*
Phase lag	4.4*	19.6*	2.7*	5.3*

d.f., degrees of freedom.
*Statistical significance at $P<0.05$.

movements of the dorsal tail-tip. In contrast, triangle D was only 8±1 % ahead of lateral movements of the dorsal tail-tip. Thus, triangles A and E achieved their maximum angle (although this is an acute angle relative to the direction of movement of the tail) as the tail crossed the midline of its path of travel (25 % of a tail-beat cycle; Fig. 12). However, the most dorsal triangle, D, achieved its maximum angle very shortly before the tail reached its maximum lateral displacement (Fig. 12). Similarly, triangles A and E were at approximately 90 ° relative to the *xz* plane shortly after the tail was maximally laterally displaced. Triangle D was not at an orientation of 90 ° until after the tail had begun to beat in the opposite direction (115 % of cycle time; Fig. 12).

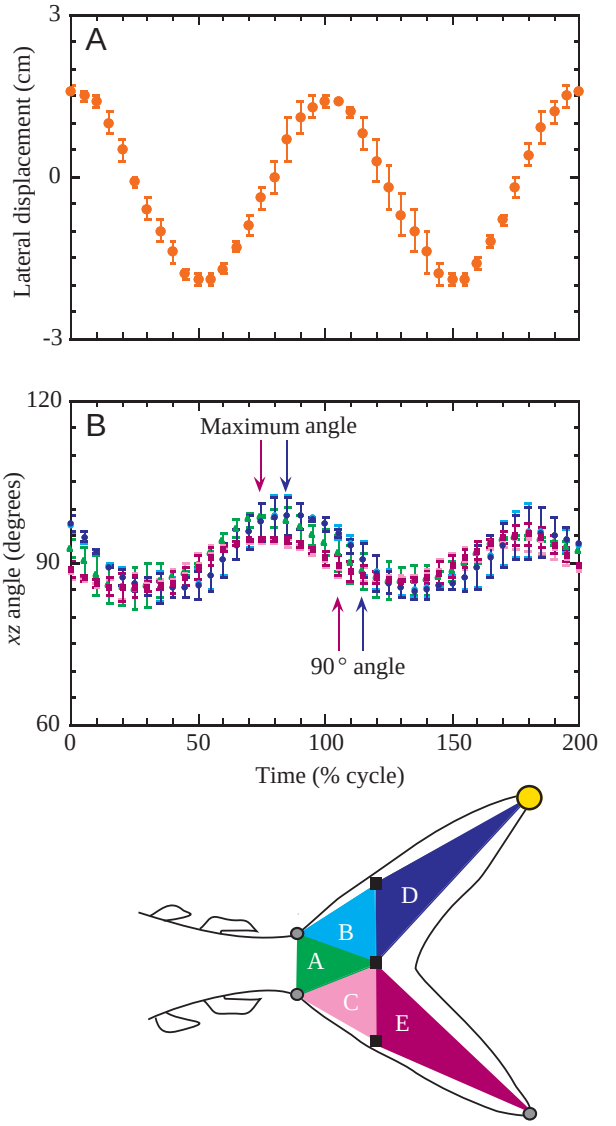

Fig. 12. Orientation of tail triangles in the *xz* plane and lateral displacement of the tail-tip during the tail-beat cycle. Points represent the mean values (±S.E.M.) for all individuals swimming at the lowest swimming speed ($1.2\,L\,s^{-1}$) for two complete tail beats. (A) Lateral displacement of the tail-tip and (B) *xz* angle of all tail triangles. Markers on the graphs are color-coded to match the tail triangles.

Discussion

Orientation of the body and pectoral fins

Qualitative observations indicated that the pectoral fins were abducted at all speeds for *S. japonicus*, but that the degree of abduction decreased with swimming speed. A decrease in pectoral fin abduction with speed has traditionally been quantified as an increase in sweepback angle (i.e. the angle of the trailing edge of the fin relative to a line perpendicular to the long axis of the body). Thus, our results for *S. japonicus* are similar to the results of a study by Dewar and Graham (1994) using yellowfin tuna (*Thunnus albacares*) swimming in a flow tunnel, which showed that sweepback angle increased linearly with swimming speed. In addition, an increase in sweepback angle with increasing speed was reported in kawakawa tuna (*Euthynnus affinis*) swimming in circular tanks (Magnuson, 1970). According to calculations by Magnuson (1970), an increase in sweepback angle in scombrids is accompanied by a decrease in the coefficient of lift for the pectoral fins. However, the lift generated by the pectoral fins will increase with increased water flow around the fins. It appears that *S. japonicus* and other scombrids decrease pectoral fin area in order to maintain constant lift as swimming speed increases.

Measurements of the body angle of *S. japonicus* indicated that chub mackerel swim tipped very slightly downwards at all swimming speeds. This result is surprising because a previous study demonstrated that *Scomber scombrus* (a sister species to *S. japonicus*) tilts its body upwards at very low ($<1.0\,L\,s^{-1}$) swimming speeds (He and Wardle, 1986). The lowest speed examined in this study was $1.2\,L\,s^{-1}$ (*S. japonicus* would not swim consistently below this speed in the flow tank); it is possible that *S. japonicus* also tip upwards at swimming speeds below $1.0\,L\,s^{-1}$. However, other researchers have suggested that there is no body tipping in other scombrids (i.e. tunas) at any voluntary swimming speed (Magnuson, 1970, 1978).

Although orientation of the body into the flow is important because it can affect the force balance on a swimming fish, body shape is also important. Previous research on the kawakawa tuna *Euthynnus affinis*, has suggested that the tuna body produces no lift at 0 ° angle of attack to the flow because it has no significant camber and a low aspect ratio (Magnuson,

1970). Although *S. japonicus* has a somewhat different body shape from that of *E. affinis*, it seems reasonable to assume that the body generates little upward lift at a 0 ° or slightly negative angles of attack. Thus, it appears that *S. japonicus* does not use body shape or orientation to generate significant vertical lift during steady swimming.

Speed effects

Previous research on fish locomotion has indicated that tail-beat amplitude increases only at very low swimming speeds (Bainbridge, 1958, 1963). However, the only other data previously collected for *S. japonicus* (Hunter and Zweifel, 1971) suggested that tail-beat amplitude does not increase with swimming speed, even when very low speeds are considered. Hunter and Zweifel (1971) also found no correlation between swimming speed and tail-beat amplitude in another species of marine teleost (*Trachurus symmetricus*), although tail-beat frequency did increase linearly in all species examined. These results led Hunter and Zweifel (1971) to propose that swimming fish increase their tail-beat amplitude only during periods of acceleration.

Our data clearly indicate that tail-beat amplitude increases with swimming speed (Table 2; Fig. 10) in *S. japonicus*. In fact, at the dorsal tail-tip, amplitude increases by 32 % between 1.2 and 3.0 $L\,s^{-1}$ (Table 2). The finding by other authors of no increase in tail-beat amplitude with swimming speed in chub mackerel may be an artifact resulting from the use of only ventral or dorsal views to measure amplitude. Since the chub mackerel tail changes shape during the tail beat, and there is significant dorso–ventral asymmetry in tail movements (see Results), it is not always possible to follow a single point on the tail throughout the beat using a ventral or dorsal silhouette of the swimming fish. Thus, changes in tail shape during swimming may mask amplitude changes with speed. When a posterior view is available (Fig. 3), specific points on the tail can be identified both throughout a beat and across speeds. This allows accurate measurement of *z* excursions for specific locations on the tail and, under these conditions, an increase in tail-beat amplitude with swimming speed can be measured.

However, it is also possible that chub mackerel tail-beat amplitude reaches a maximum at 3.0 $L\,s^{-1}$ and would not increase with further increases in swimming speed. The data of Bainbridge (1958) for swimming goldfish (*Carassius auratus*) suggest that amplitude increases when tail-beat frequency is below 4 Hz, and above this frequency it will not increase further. Tail-beat frequency at the highest swimming speed for *S. japonicus* was just under 4 Hz; thus, any plateau in amplitude for this species could occur at higher swimming speeds and higher tail-beat frequencies.

Mackerel tail function

Planar angles of the tail triangles (representative of the caudal fin surface) were used to determine the three-dimensional orientation of the tail during the tail beat. The *xz* angle is the most important planar angle for testing the hypothesis that the tail of *S. japonicus* functions with dorso–ventral symmetry. As the tail oscillates laterally, the *yz* angle will oscillate above and below 90 ° and the *xy* angle will oscillate above and below 0 °. However, no such change is obligate in the *xz* plane. If the tail functions in a dorso–ventrally symmetrical manner with no bending out of the vertical plane, then the *xz* angle could be 90 ° during most (or all) of the tail beat (as shown for angle β for the homocercal model in Fig. 1). However, this is not the pattern we observed. Our data indicate that the tail is not perpendicular to the *xz* plane during most of the tail beat (Fig. 12). In fact, as it crosses the midline, the tail subtends an angle of approximately 80 ° relative to its direction of travel in the *xz* plane. In addition, homologous dorsal and ventral tail triangles sometimes demonstrate different *xz* orientations. For example, the *xz* angles of the triangles on the dorsal and ventral lobes (triangles D and E) are slightly out of phase with one another (Fig. 12; Table 3). Clearly, the tail of *S. japonicus* does not function according to the traditional homocercal model.

Previous research on swimming tunas has suggested that the caudal peduncle leads the tail during the tail beat in scombrid fishes (Fierstine and Walters, 1968). This pattern of tail movement has been used to contrast scombrids with more generalized teleosts in which the dorsal-most and ventral-most fin rays are purported to lead the tail during the beat (Bainbridge, 1963; Webb, 1975). In the present study, the three-dimensional angles can be used to assess which portion of the tail 'leads' during the beat.

The *xz* angle is the best indicator of the orientation of the tail relative to its direction of travel (since most movement during the beat occurs in the *z*, or lateral, dimension). If the caudal peduncle leads the tail, then the dorsal and ventral tips of the tail should trail behind the central region. If the tail functions in this manner, then the *xz* angle of the upper tail triangle (D) should be obtuse (>90 °) relative to its direction of movement because both lobes of the tail will be deflected away from the peduncle by water resistance (although the ventral lobe would form an acute angle for the same reason). In fact, both the dorsal and ventral posterior lobes form acute *xz* angles (<90 °) relative to the direction of tail movement during most of the tail beat (Fig. 12). This suggests that the central region does not lead the dorsal and ventral portions of the tail in *S. japonicus* as the tail moves laterally. Instead, the tail moves as a single-angled blade for most of the tail beat, as demonstrated by the three-dimensional angles measured for the tail triangles (Figs 11, 12).

However, in one sense, the caudal peduncle will always 'lead' the tail-tips because of the posterior propagation of the wave of bending. As this wave travels posteriorly along the fish, the caudal peduncle region will consistently reach its maximum lateral displacement slightly ahead of the posterior regions of the tail (e.g. Fig. 10; points 1 and 2 on the caudal peduncle are consistently ahead of point 6 on the ventral tail-tip). This phenomenon may have led to confusion in previous two-dimensional studies of tail movements.

A few researchers (Aleev, 1969; He and Wardle, 1986) have suggested that mackerel may generate asymmetrical tail

movements during steady swimming, but this was generally believed to occur only at very low swimming speeds (Videler, 1993). A study of *S. scombrus* swimming back and forth in a rectangular chamber (He and Wardle, 1986) reported dorso–ventral tail asymmetry at speeds below $1.0\,L\,s^{-1}$; however, at those speeds, *S. scombrus* also tipped its body up into the flow while swimming (see above). Videler (1993) suggested that four forces acting on the fish combine to produce a stable vertical position in the water column (i.e. no rising or sinking). First, the body of a mackerel is negatively buoyant (Magnuson, 1973), and this tends to move the fish towards the substratum. Second, the pectoral fins are unable to produce significant lift at very low speeds because of the low flow velocity over the fin surface (Magnuson, 1973). Third, the body is tipped up to provide additional upward lift for the anterior portion of the fish. Finally, the tail is oscillated asymmetrically (with the dorsal lobe leading) and produces upward lift to balance the lift generated anteriorly. This theory has led to two predictions about dorso–ventral asymmetrical tail movements: (1) this phenomenon will not occur in mackerel swimming at high speeds, and (2) neutrally buoyant fish will not demonstrate this phenomenon (Videler, 1993).

By combining our data with other recent studies, we can address both these predictions. First, our data for *Scomber japonicus* swimming from $1.2–3.0\,L\,s^{-1}$ show that dorso–ventral asymmetry is present in the tail at all swimming speeds. In fact, there is no measurable change in the degree of tail dorso–ventral asymmetry as speed increases (Table 3). Second, recent research has suggested that significant dorsal–ventral asymmetry and tilting at low speeds may also be present in other teleosts with near-neutral buoyancy (Lauder, 1989, 1999; Webb, 1993). These results cast doubt on the theory that asymmetrical tail movements are associated only with low swimming speeds and negatively buoyant fishes to balance lift generated by body tilting.

Perhaps the most accurate previous description of mackerel tail movements was made 30 years ago by Aleev (1969) on the basis of previously published still images of swimming mackerel. Aleev (1969) suggested that, since *Scomber* sp. is slightly negatively buoyant, the tail produces lift to keep the fish from sinking. Vertical lift produced posteriorly by the tail may be balanced by anterior lift generated by the pectoral fins. Aleev (1969) suggested that mackerel tails always subtend an acute angle relative to their direction of movement and proposed a schematic model of *Scomber* tail movements that is strikingly similar to our results (see Fig. 35 in Aleev, 1969). In addition, Aleev (1969) pointed out that Gray (1933), in his classic paper on fish swimming, included an image of *Scomber scombrus* swimming. Although that picture is only a dorsal view of a swimming mackerel, it clearly demonstrates that the dorsal and ventral tail-tips are not moving synchronously during the tail beat.

Comparisons with other scombrids

The only other analysis of the tail angle from a posterior view in a scombrid is given in Magnuson (1970) for the kawakawa tuna *Euthynnus affinis*. Magnuson and his colleagues found that the 'average' value of the tail angle was 89 ° during the tail-beat cycle. Magnuson (1970) interpreted this as evidence that the tail is dorso–ventrally symmetrical and creates no posterior lift during the beat. Magnuson's hydrodynamic calculations instead suggest that the wing-like keel creates lift in the posterior region of tunas. In fact, the keel is poorly developed in *S. japonicus*, and this could potentially lead to differences in tail kinematics between tunas and mackerels. However, there are two potential problems with the angle measurement for *E. affinis*. First, they are two-dimensional angles measured from a rear view of the tail in fish swimming away from a camera, and other work has demonstrated that two-dimensional angle calculations can be misleading (Lauder and Jayne, 1996; Lauder, 1999). Second, the relevance of an 'average' value for this angle is not clear. In *S. japonicus*, this angle varies cyclically through time (Fig. 12) and an 'average' value will be affected by the phase of the tail-beat cycle that is sampled. More research specifically examining the three-dimensional movements of swimming tunas is necessary to determine whether tunas and mackerels are similar in their tail kinematics.

Muscular control of tail movements

The results of this study suggest that there is fine control of the tail during the tail-beat cycle. For example, the tail is vertically expanded and compressed during the tail-beat cycle (Fig. 7). Previous researchers (Bainbridge, 1963; Webb, 1975) have suggested that tail span and area (and thus aspect ratio) change during a tail beat in fishes. Bainbridge (1963) showed a cyclical pattern of expansion and compression for the dace *Leuciscus leuciscus*, but he did not propose a specific mechanism for this behavior. In *S. japonicus*, the change in tail size is also cyclical and demonstrates the same pattern as seen in Bainbridge's (1963) data: expansion of the tail in *S. japonicus* is minimal at extreme lateral positions and maximal when crossing the midline (Fig. 7). These changes in tail height (and consequently tail area) will maximize the surface area and velocity of the tail when it exerts force on the water and minimize drag on the tail during the transition between beats (Bainbridge, 1963; Lauder, 1999).

It is possible that cyclical vertical compression of the tail is generated *via* action of the interradialis muscle, which is positioned such that contraction of this muscle could draw the dorsal and ventral fin rays towards one another (Fig. 5). Physical manipulation of preserved specimens suggests that most of the flexibility that exists in the tail is located along the posterior edge of the fork where the upper and lower fin rays meet (Fig. 5). Although it is possible that the vertical compression of the caudal fin is due to activity of the interradialis muscle, at this time we cannot rule out the possibility of passive compression of the tail resulting from the force of water on the fin rays. In addition, there is no obvious active mechanism for the vertical expansion of the fin (Fig. 5);

expansion may be caused passively by the resistance of the water to the tail movements.

The extreme internal and external morphological symmetry of the caudal fin in *S. japonicus* (Fig. 5) suggests that an active mechanism is responsible for the dorso–ventral asymmetry present in the fin during the tail-beat cycle. However, the exact mechanism is unknown. Recent research on another derived teleost, the bluegill sunfish *Lepomis macrochir* (Lauder, 1999), has suggested that the hypochordal longitudinalis is responsible for lateral bending of the dorsal fin rays during the tail beat. Although it has previously been reported as only 'a tendinous remnant' in scombrids (Fierstine and Walters, 1968), this muscle is present in *S. japonicus* (Fig. 5) and it is oriented such that it could potentially act on the dorsal fin rays. However, this muscle is very small in *S. japonicus*, and it is certainly possible that the muscle is vestigial, as has been suggested previously (Fierstine and Walters, 1968).

An alternative hypothesis is that the dorso–ventral asymmetry in the caudal fin is generated by the axial musculature and transmitted to the tail. Future experiments using electromyography could determine whether the hypochordal longitudinalis muscle is active during steady swimming in *S. japonicus* and whether its activity pattern correlates with changes in the orientation of the upper lobe of the tail. If this muscle is not active during steady swimming, then the axial musculature may be responsible for determining tail orientation.

However, one line of evidence that supports the hypothesis that the anterior musculature generates asymmetrical tail movements can be obtained from the present study by comparing the orientations of the triangles defined on the tail. The magnitude of the maximum/minimum *xz* angle of triangle A, located on the caudal peduncle, is not significantly different from the maximum/minimum *xz* angle of triangles D and E (Fig. 12, Table 3). This result implies that dorso–ventral asymmetry is imparted to the tail anterior to the caudal peduncle. This, in turn, suggests that the axial musculature generates asymmetry and that the intrinsic musculature of the tail may not contribute significantly to this effect.

Future research

Our results clearly indicate that tail movements of *S. japonicus* do not follow the classic homocercal tail model. Instead, the tail of *S. japonicus* demonstrates consistent dorso–ventral asymmetry and oscillates laterally as an acutely angled blade during much of the tail beat. However, several additional questions about tail function remain unanswered.

First, the presence of dorso–ventral asymmetry suggests that water is deflected downwards during the tail beat. Ventral deflection of the water should exert a reaction force on the tail that will push the tail upwards and forwards. Lift generated by the pectoral fins, and the tendency of a negatively buoyant body to sink, could potentially balance this vertical force. This force balance is similar to that traditionally predicted for the heterocercal tail model (Fig. 1). However, careful studies of the flow of water around the fins of a swimming mackerel are necessary both to describe and to understand force balance on the fish during steady swimming.

Second, the role of muscles in producing complex tail movements should be examined. Two types of movement are of particular interest: (1) expansion and compression of the tail during the tail beat, and (2) dorso–ventral asymmetry of tail movements. Studies examining activity patterns of both the axial musculature and the intrinsic tail musculature are necessary to determine what active and passive forces are involved in creating these surprisingly complex tail movements.

This project was supported by NSF DBI-9750303 to A.C.G., NSF IBN 93-18065 to K.A.D. and NSF IBN 98-07012 to G.V.L. We thank Jeanine Donley and Chugey Sepulveda for assistance in obtaining, transporting and videotaping mackerel. In addition, we thank several anonymous reviewers for their helpful comments on the manuscript.

References

Affleck, R. J. (1950). Some points in the function, development and evolution of the tail in fishes. *Proc. Zool. Soc., Lond.* **120**, 349–368.

Ahlborn, F. (1896). Über die Bedeutung der Heterozerkie und ähnlicher unsymmetrischer Schwanzformen schwimmender Wirbeltiere für die Ortsbewegung. *Z. Wiss. Zool.* **61**, 1.

Aleev, Y. G. (1969). *Function and Gross Morphology in Fish*. Jerusalem: Keter Press.

Alexander, R. McN. (1965). The lift produced by the heterocercal tails of Selachii. *J. Exp. Biol.* **43**, 131–138.

Bainbridge, R. (1958). The speed of swimming fish as related to size and to the frequency and amplitude of the tail beat. *J. Exp. Biol.* **35**, 109–133.

Bainbridge, R. (1963). Caudal fin and body movements in the propulsion of some fish. *J. Exp. Biol.* **40**, 23–56.

Beamish, F. W. H. (1978). Swimming capacity. In *Fish Physiology*, vol. VII, Locomotion (ed. W. S. Hoar and D. J. Randall), pp. 101–187. New York: Academic Press.

Breder, C. M. (1926). The locomotion of fishes. *Zoologica* **4**, 159–256.

Dewar, H. and Graham, J. B. (1994). Studies of tropical tuna swimming performance in a large water tunnel. III. Kinematics. *J. Exp. Biol.* **192**, 45–59.

Ferry, L. A. and Lauder, G. V. (1996). Heterocercal tail function in leopard sharks: a three-dimensional kinematic analysis of two models. *J. Exp. Biol.* **199**, 2253–2268.

Fierstine, H. L. and Walters, V. (1968). Studies in locomotion and anatomy of scombroid fishes. *Mem. S. Calif. Acad. Sci.* **6**, 1–31.

Gosline, W. A. (1971). *Functional Morphology and Classification of Teleostean Fishes*. Honolulu: University of Hawaii Press.

Gray, J. (1933). Studies in animal locomotion. I. The movements of fish with special reference to the eel. *J. Exp. Biol.* **10**, 88–104.

Grove, A. J. and Newell, G. E. (1936). A mechanical investigation into the effectual action of the caudal fin of some aquatic chordates. *Ann. Mag. Nat. Hist.* **11**, 280–290.

He, P. and Wardle, C. S. (1986). Tilting behavior of the Atlantic mackerel, *Scomber scombrus*, at low swimming speeds. *J. Fish Biol.* **29**, 223–232.

Hunter, J. R. and Zweifel, J. R. (1971). Swimming speed, tail beat frequency, tail beat amplitude and size in jack mackerel, *Trachurus symmetricus* and other fishes. *Fishery Bull.* **69**, 253–266.

Lauder, G. V. (1989). Caudal fin locomotion in ray-finned fishes: Historical and functional analyses. *Am. Zool.* **29**, 85–102.

Lauder, G. V. (1999). Function of the caudal fin during locomotion in fishes: kinematics, flow visualization, and evolutionary patterns. *Am. Zool.* (in press).

Lauder, G. V. and Jayne, B. C. (1996). Pectoral fin locomotion in fishes: testing drag-based models using three-dimensional kinematics. *Am. Zool.* **36**, 567–581.

Magnuson, J. J. (1970). Hydrostatic equilibrium of *Euthynnus affinis*, a pelagic teleost without a gas bladder. *Copeia* **1**, 56–85.

Magnuson, J. J. (1973). Comparative study of adaptations for continuous swimming and hydrostatic equilibrium of scombrid and xiphoid fishes. *Fishery Bull.* **71**, 337–356.

Magnuson, J. J. (1978). Locomotion by scombrid fishes: Hydrodynamics, morphology and behavior. In *Fish Physiology*, vol. VII (ed. W. S. Hoar and D. J. Randall), pp. 240–315. New York: Academic Press.

Nursall, J. R. (1963). The caudal musculature of *Hoplopagrus guntheri* Gill (Perciformes: Lutjanidae). *Can. J. Zool.* **41**, 865–880.

Patterson, C. (1968). The caudal skeleton in lower Liassic pholidophorid fishes. *Bull. Br. Mus. Nat. Hist. Geol.* **16**, 203–239.

Schulze, F. E. (1894). Über die Abwärtsbeugung des Schwantzteiles der Wirbelsäule bei Ichthyosauren. *Sitzungsber. Akad. Wiss. Berlin* **43–44**.

Videler, J. J. (1993). *Fish Swimming*. London: Chapman & Hall.

Webb, P. W. (1975). Hydrodynamics and energetics of fish propulsion. *Bull. Fish. Res. Bd Can.* **190**, 1–159.

Webb, P. W. (1993). Is tilting at low speeds unique to negatively buoyant fishes? Observations on steelhead trout, *Oncorhynchus mykiss* and bluegill, *Lepomis macrochirus*. *J. Fish Biol.* **43**, 687–694.

Zar, J. H. (1984). *Biostatistical Analysis*. Englewood Cliffs: Prentice-Hall.